THEORETICAL INORGANIC CHEMISTRY

Hexagonal borophene stabilized by mixed doping: Structure, stability, electronic and mechanical properties

D. V. Steglenko[a,*], T. N. Gribanova[a], R. M. Minyaev[a]

[a] *Southern Federal University, Institute of Physical and Organic Chemistry, Rostov-on-Don, 344090 Russia*

Received July 08, 2024
Revised September 09, 2024
Accepted September 11, 2024

Using DFT calculations, the possibility of stabilizing the hexagonal honeycomb shape of borophene by mixed doping in the $B_6Ga_2Mg_4$ system was showed, where a flat sheet of borophene is placed between two layers formed by magnesium and gallium atoms. $B_6Ga_2Mg_4$ is a relatively soft material with metallic conductivity. Evaluation of the thermodynamic stability of this compound shows that melting will occur at temperatures above 1200 °K.

Keywords two-dimensional materials, DFT calculations, band structure, mechanical properties, thermal stability

DOI: 10.31857/S0044457X250108e9

INTRODUCTION

Currently, two-dimensional (**2D**) materials have attracted much attention due to their unusual physical and chemical properties [1, 2]. Due to their reduced dimensionality and the possibility of additional functionalization, they acquire such improved properties as a reduced tendency to coagulation, chemical stability, and manufacturability [3], and can find application as electronic or optoelectronic devices [4–7], in spintronics [8, 9], as well as in solar cell elements, catalysts, electric energy storage devices, and sensor devices [3, 10, 11]. Of particular interest are two-dimensional systems constructed from boron atoms that have a honeycomb structure [12–15], since it is assumed that it is the boron hexagonal sublattice that is responsible for superconductivity in MgB_2[16–18] However, due to the lack of electrons onp_z-orbitals, the two-dimensional boron sheet with a honeycomb structure

exhibits lattice instability, so the issue of stabilizing the hexagonal boron structure is of primary importance.

An effective way to stabilize non-standard boron forms, such as fullerenes, extended boron chains, etc., is doping, which can be carried out using atoms of both metals and non-metals [19-23]. A two-dimensional boron lattice with a honeycomb structure can be stabilized by donating electron density to p_z -orbitals through doping with alkali and alkaline earth metal atoms [24] or self-doping [25]. Studies have shown that polymorphic modifications of two-dimensional boron sheets arising in the case of self-doping can possess superconducting properties with a temperature $T_c \sim 10 - 20\,\mathrm{K}$ [26]. Modifications of the donor system allow controlling the properties and stability of borophene derivatives, and the study of methods for stabilizing two-dimensional boron sheets with a hexagonal lattice opens up new possibilities for obtaining materials with technologically useful properties. Previously [27], we proposed a method for stabilizing a hexagonal boron lattice by bilateral doping, where sodium was considered as an electron donor. This paper presents a theoretical study of the three-layer system $B_6Ga_2Mg_4$ (Fig. 1), in which the stabilization of a flat borophene sheet is provided by bilateral doping as a result of its placement between two layers of mixed composition formed by Ga and Mg atoms.

THEORETICAL PART

Calculations in the two-dimensional infinite crystal approximation were performed using the VASP (Vienna Ab initio Simulation Package) software [28–31] with the PBE functional [32] and PAW pseudopotentials (GW version) [33, 34]. In all calculations, the plane wave energy was 550 eV, the wave function minimization threshold was set at 1×10^{-8} eV, and residual gradients on atoms were less than 1×10^{-4} eV/Å. Brillouin zone discretization was performed using the Monkhorst-Pack method [35] with an automatically generated 15 × 15 × 1 grid. The phonon spectrum

was calculated using the Phonopy program [36] for a 6 × 6 × 1 supercell. For band structure calculations, the Brillouin zone discretization was increased to 31 × 31 × 1. To reduce the influence of adjacent layers on each other, an interlayer distance of >13 Å was established. To evaluate the thermal stability of $B_6Ga_2Mg_4$, molecular dynamics (**MD**) calculations were performed in the canonical (NVT) ensemble approximation at temperatures of 1000, 1200, and 1300 K. For this, a 4 × 4 × 1 supercell was used, and the Brillouin zone discretization was set as 1 × 1 × 1. In all MD calculations, the plane wave energy was 550 eV. Temperature control was carried out according to the Nosé thermostat scheme [37]. The Vesta program [38] was used to visualize the studied systems. The spatial symmetry group was determined using the ISOTROPY (FINDSYM) software package [39].

RESULTS AND DISCUSSION

As calculation results show, the optimized crystal structure has a hexagonal system and belongs to the space group *P* 6/ *mmm* (191). Table 1 shows the lengths of the corresponding Bravais lattice vectors, the coordinates of atoms in the unit cell, and Wyckoff positions for gallium, magnesium, and boron atoms. Figure 2 shows the spatial structure of $B_6Ga_2Mg_4$.

The Bravais lattice basis consists of six boron atoms, two gallium atoms, and four magnesium atoms with a stoichiometric ratio of 1 : 2 : 3 (Ga : Mg : B). The boron atoms form a perfectly flat hexagonal lattice located between two heteroatomic layers, in which gallium and magnesium atoms are positioned apically on both sides relative to the centers of boron hexagons. The calculated B–Ga and B–Mg distances are 2.598 and 2.453 Å. The boron lattice has two types of bonds: the bond length between boron atoms forming a cycle, above which a gallium atom is located, is 1.754 Å, and the lengths of B–B bonds connecting boron cycles with apical gallium atoms are 1.775 Å (Fig. 2). Such exocyclic B–B bonds slightly (0.025 Å) exceed the

sum of covalent radii of boron atoms, while endocyclic bonds are essentially equal to the length of a single B–B bond (1.75 Å [40]). At the same time, the B–Ga and B–Mg distances exceed the sum of the covalent radii of B–Ga by 0.468 Å ($d_{cov} = 2.130$ Å) and B–Mg by 0.213 Å ($d_{cov} =$ 2.224 Å). The distances between adjacent magnesium atoms are 3.051 Å, which exceeds the sum of covalent radii ($d_{cov} = 2.720$ Å) by 0.331 Å. The Ga–Mg distance is practically equal to the Mg–Mg distance and is 3.058 Å, which exceeds the sum of covalent radii ($d_{cov} = 2.61$ Å) by 0.448 Å.

To assess the dynamic stability of the two-dimensional borographene system, we calculated the phonon spectrum (Fig. 3). The calculation results show that there are no dispersion curves in the imaginary region of the phonon spectrum, i.e., the structure under consideration is dynamically stable. The phonon spectrum notably lacks an energy gap between acoustic and optical branches.

Calculations of the electronic band structure of $B_6Ga_2Mg_4$ along high-symmetry directions of the Brillouin zone show that such a compound should possess metallic properties (Fig. 4). Thus, there is no band gap, and the conduction band and valence band cross the Fermi level ($E = 0$). Therefore, similar to two-dimensional sodium-doped borophene [27], $B_6Ga_2Mg_4$ will also be a metal.

Figures 5–7 show the partial densities of electronic states formed by boron, gallium, and magnesium atoms.

As can be seen from Fig. 5, in $B_6Ga_2Mg_4$ the zone located below the Fermi level is formed mainly by *p* -orbitals of boron atoms. To a lesser extent, *p* -orbitals of gallium atoms are represented here (Fig. 6). At the same time, the main contribution from magnesium atoms to the formation of the zone lying above the Fermi level comes from *s* -orbitals, while the contribution of *p* -orbitals is quite insignificant (Fig. 7).

The conduction band is formed mainly by *p* -orbitals of boron and gallium atoms, and the contributions of *p* -orbitals of these atoms are comparable (Fig. 5 and 6). To

a lesser extent, *s* -and *p* -orbitals of magnesium atoms participate in the formation of the conduction band.

Using DFT calculations, we determined the criterion of mechanical stability of two-dimensional $B_6Ga_2Mg_4$, as well as Young's modulus and Poisson's ratio, which characterize the measure of rigidity and transverse deformation during compression or tension of a solid body. In the case of hexagonal systems, the necessary and sufficient criterion for mechanical stability is defined as follows [41]: $c_{11} > |c_{12}|$, $2c_{13}^2 < c_{33}(c_{11} + c_{12})$, $c_{44} > 0$. In the two-dimensional case, the above inequalities for the components of the elasticity tensor take the form: $c_{11} > |c_{12}|$, $c_{66} > 0$. The calculated values of elastic constants are presented in Table 2. For a transversely isotropic material, Young's modulus can be calculated using the formula: $Y_x = (c_{11}-c_{12}) \cdot ((c_{22} + c_{21}) \cdot c_{33} - 2c_{13}^2)/c_{22} \cdot c_{33} - c_{13}^2$ [42]. In the case of a two-dimensional transversely isotropic material, we get: $Y_{2D} = c_{11}^2 - c_{12}^2/c_{11}$. Similarly, the Poisson's ratio is defined as $v = c_{12}/c_{11}$ [43, 44].

From the data presented in Table 2, it can be seen that the calculated Young's modulus (Y_{2D}) for $B_6Ga_2Mg_4$ is 139.6 N/m, which is significantly lower than for graphene (340 ± 50 N/m) [46, 47] and two-dimensional boron nitride *hex* -BN (289 ± 24 N/m) [49], however it is comparable to two-dimensional MoS_2 (180 ± 60, 130 N/m) [50, 51] and slightly higher than sodium-doped borophene B_2Na_2 [27] or silicene monolayer (62 N/m) [52, 55]. In terms of mechanical properties, $B_6Ga_2Mg_4$ is similar to two-dimensional B_4P_2 and B_4As_2, for which Y_{2D} = 142.5 and 130.4 N/m respectively [52, 53]. Thus, the theoretically predicted $B_6Ga_2Mg_4$ is a relatively soft material. The low value of Poisson's ratio indicates that under uniaxial tension or compression, the transverse deformation of the $B_6Ga_2Mg_4$ monolayer will be comparable to two-dimensional *hex* -BN.

Table 3 shows the calculated energy values of boron, gallium, magnesium atoms and two-dimensional $B_6Ga_2Mg_4$. For isolated atoms, spin-polarized DFT calculations were performed using the broken symmetry method.

The formation energy was calculated using the formula:

$$E_f = \frac{E_{B_6Ga_2Mg_4} - (6E_B + 2E_{Ga} + 4E_{Mg})}{n},$$

where $n = 1$ in the case of E_{f1} and $n = 12$ in the case of E_{f2}.

As follows from Table 3, the predicted two-dimensional $B_6Ga_2Mg_4$ should be a relatively stable compound, with thermodynamic stability higher than that of sodium-doped two-dimensional borophene (3.54 eV/atom) [27].

To assess the thermal stability, quantum-chemical modeling of the melting process of the $B_6Ga_2Mg_4$ sheet was performed using the MD method. In all MD calculations, the integration step was 3 fs, and the total trajectory in phase space was 10.5 ps (3500 steps). For modeling the melting process, a 4 × 4 × 1 supercell containing 192 atoms was used. A series of calculations carried out at different temperatures showed that the $B_6Ga_2Mg_4$ sheet maintains its stability at 1200 K (Fig. 8).

To track the melting process, a pair correlation function was used, reflecting the degree of long-range order in the substance [56]. During the solid-liquid phase transition, the peaks corresponding to the presence of long-range order disappear, indicating melting [57], which occurs in the two-dimensional $B_6Ga_2Mg_4$ sheet at 1300 K (Fig. 8). The broadening and reduction of peaks are due to the increase in the amplitude of thermal vibrations, which distort the structure (Fig. 8c), however, melting does not occur (at least at 1200 K).

From the graph of the pair correlation function (Fig. 8a), it can be concluded that the onset of melting occurs at a temperature of ~1300 K. This is indicated by the broadening and reduction of peaks, which signifies a sharp decrease in long-range order in the solid. This is also noticeable in the significant distortion of the structure

of two-dimensional $B_6Ga_2Mg_4$ (Fig. 8d). At the same time, MD modeling at temperatures of 1000 and 1200 K for 10.5 ps showed that despite significant distortions, the overall structure of the two-dimensional $B_6Ga_2Mg_4$ sheet is preserved (Fig. 8b, 8c). From this, it can be concluded that the thermal stability of $B_6Ga_2Mg_4$ should be maintained up to a temperature of ~1200 K. Thus, $B_6Ga_2Mg_4$ is thermally more stable compared to the previously studied Na-doped borophene [27], which is stable at temperatures <200 K.

CONCLUSION

Using quantum-chemical modeling by the DFT method, the spatial and electronic structure was studied, the dynamic and thermal stability, the criterion of mechanical stability were evaluated, Young's modulus and Poisson's ratio were calculated for a two-dimensional boron sheet with a honeycomb structure doped with magnesium and gallium atoms. The obtained results show that the $B_6Ga_2Mg_4$ system is stable, possesses metallic properties, and high thermal stability. The results of the mechanical properties analysis show that such a compound should be relatively soft and resemble two-dimensional MoS_2. Thus, mixed doping is an effective way to stabilize the hexagonal structure of borophene, allowing for directed regulation of its stability and properties.

FUNDING

This work was supported by the Russian Science Foundation (grant No. 23-23-00338).

CONFLICT OF INTEREST

The authors declare that they have no conflict of interest.

REFERENCES

1. *Novoselov K.S., Geim A.K., Morozov S.V. et al.* // Science. 2004. V. 306. № 5696. P. 666. https://doi.org/10.1126/science.1102896
2. *Castro Neto A.H., Guinea F., Peres N.M.R. et al.* // Rev. Mod. Phys. 2009. V. 81. № 1. P. 109. https://doi.org/10.1103/RevModPhys.81.109
3. *Yang X., Xu M., Qiu W. et al.* // J. Mater. Chem. 2011. V. 21. № 22. P. 8096. https://doi.org/10.1039/c1jm10697j
4. *Wang Q.H., Kalantar-Zadeh K., Kis A. et al.* // Nat. Nanotechnol. 2012. V. 7. № 11. P. 699. https://doi.org/10.1038/nnano.2012.193
5. *Radisavljevic B., Radenovic A., Brivio J. et al.* // Nat. Nanotechnol. 2011. V. 6. № 3. P. 147. https://doi.org/10.1038/nnano.2010.279
6. *Chen Y.L., Analytis J.G., Chu J.-H. et al.* // Science. 2009. V. 325. № 5937. P. 178. https://doi.org/0.1126/science.1173034
7. *Jariwala D., Sangwan V.K., Lauhon L.J. et al.* // ACS Nano. 2014. V. 8. № 2. P. 1102. https://doi.org/10.1021/nn500064s
8. *Miao N., Xu B., Bristowe N.C. et al.* // J. Am. Chem. Soc. 2017. V. 139. № 32. P. 11125. https://doi.org/10.1021/jacs.7b05133
9. *Kumar H., Frey N.C., Dong L. et al.* // ACS Nano 2017. V. 11. № 8. P. 7648. https://doi.org/10.1021/acsnano.7b02578
10. *Tan C., Cao X., Wu X.-J. et al.* // Chem. Rev. 2017. V. 117. № 9. P. 6225. https://doi.org/10.1021/acs.chemrev.6b00558
11. *Xu M., Liang T., Shi M. et al.* // Chem. Rev. 2013. V. 113. № 5. P. 3766. https://doi.org/10.1021/cr300263a
12. *Gribanova T.N., Minyaev R.M., Minkin V.I. et al.* // Struct. Chem. 2020. V. 31. № 6. P. 2105. https://doi.org/10.1007/s11224-020-01606-9
13. *Kaneti Y.V., Benu D.P., Xu X. et al.* // Chem. Rev. 2022. V. 122. № 1. P. 1000. https://doi.org/10.1021/acs.chemrev.1c00233
14. *Yadav S., Sadique M.A., Kaushik A. et al.* // J. Mater. Chem. B. 2022. V. 10. № 8. P. 1146. https://doi.org/10.1039/d1tb02277f
15. *Wang Z.-Q., Lü T.-Y., Wang H.-Q. et al.* // Front. Phys. 2019. V. 14. № 3. P. 33403. https://doi.org/10.1007/s11467-019-0884-5
16. *An J.M., Pickett W.E.* // Phys. Rev. Lett. 2001. V. 86. № 19. P. 4366. https://doi.org/10.1103/PhysRevLett.86.4366
17. *Kortus J., Mazin I.I., Belashchenko K.D. et al.* // Phys. Rev. Lett. 2001. V. 86. № 20. P. 4656. https://doi.org/10.1103/PhysRevLett.86.4656
18. *Choi H.J., Roundy D., Sun H. et al.* // Nature. 2002. V. 418. № 6899. P. 758. https://doi.org/10.1038/nature00898

19. *Gribanova T.N., Minyaev R.M., Minkin V.I.* // Chem. Phys. 2019. V. 522. P. 44. https://doi.org/https://doi.org/10.1016/j.chemphys.2019.02.008
20. *Gribanova T.N., Minyaev R.M., Minkin V.I.* // Struct. Chem. 2018. V. 29. № 1. P. 327. https://doi.org/10.1007/s11224-017-1031-y
21. *Gribanova T.N., Minyaev R.M., Minkin V.I.* // Struct. Chem. 2017. V. 28. № 2. P. 357. https://doi.org/10.1007/s11224-016-0886-7
22. *Gribanova T.N., Minyaev R.M., Minkin V.I.* // Mendeleev Commun. 2016. V. 26. № 6. P. 485. https://doi.org/https://doi.org/10.1016/j.mencom.2016.11.008
23. *Steglenko D.V., Gribanova T.N., Minyaev R.M.* // J. Phys. Chem. C. 2023. V. 127. № 31. P. 15533. https://doi.org/10.1021/acs.jpcc.3c02427
24. *John D., Nharangatt B., Chatanathod R.* // J. Mater. Chem. C. 2019. V. 7. № 37. P. 11493. https://doi.org/10.1039/c9tc03628h
25. *Tang H., Ismail-Beigi S.* // Phys. Rev. B. 2009. V. 80. № 13. P. 134113. https://doi.org/10.1103/PhysRevB.80.134113
26. *Penev E.S., Kutana A., Yakobson B.I.* // Nano Lett. 2016. V. 16. № 4. P. 2522. https://doi.org/10.1021/acs.nanolett.6b00070
27. *Steglenko D.V., Gribanova T.N., Minyaev R.M. et al.* // Russ. J. Inorg. Chem. 2023. V. 68. P. 60. https://doi.org/10.1134/s0036023622601477
28. *Kresse G., Hafner J.* // Phys. Rev. B. 1993. V. 47. № 1. P. 558. https://doi.org/10.1103/PhysRevB.47.558
29. *Kresse G., Hafner J.* // Phys. Rev. B. 1994. V. 49. № 20. P. 14251. https://doi.org/10.1103/PhysRevB.49.14251
30. *Kresse G., Furthmüller J.* // Phys. Rev. B. 1996. V. 54. № 16. P. 11169. https://doi.org/10.1103/PhysRevB.54.11169
31. *Kresse G., Furthmüller J.* // Comput. Mater. Sci. 1996. V. 6. №. 1. P. 15. https://doi.org/10.1016/0927-0256(96)00008-0
32. *Perdew J.P., Burke K., Ernzerhof M.* // Phys. Rev. Lett. 1996. V. 77. № 18. P. 3865. https://doi.org/10.1103/PhysRevLett.77.3865
33. *Blöchl P.E.* // Phys. Rev. B. 1994. V. 50. № 24. P. 17953. https://doi.org/10.1103/PhysRevB.50.17953
34. *Kresse G., Joubert D.* // Phys. Rev. B. 1999. V. 59. № 3. P. 1758. https://doi.org/10.1103/PhysRevB.59.1758
35. *Monkhorst H.J., Pack J.D.* // Phys. Rev. B. 1976. V. 13. № 12. P. 5188. https://doi.org/10.1103/PhysRevB.13.5188
36. *Togo A., Tanaka I.* // Scripta Mater. 2015. V. 108. P. 1. https://doi.org/10.1016/j.scriptamat.2015.07.021

37. *Nosé S.* // J. Chem. Phys. 1984. V. 81. № 1. P. 511. https://doi.org/10.1063/1.447334
38. *Koichi M., Fujio I.* // J. Appl. Crystallogr. 2011. V. 44. № 6. P. 1272. https://doi.org/10.1107/S0021889811038970
39. *Stokes H.T., Hatch D.M.* // J. Appl. Crystallogr. 2005. V. 38. № 1. P. 237. https://doi.org/10.1107/S0021889804031528
40. *Emsley J.* The elements. Oxford, 1991.
41. *Mouhat F., Coudert F.-X.* // Phys. Rev. B. 2014. V. 90. № 22. P. 224104. https://doi.org/10.1103/PhysRevB.90.224104
42. *Lubarda V.A., Chen M.C.* // J. Mech. Mater. Struct. 2008. V. 3. № 1. P. 153. https://doi.org/10.2140/jomms.2008.3.153
43. *Wei X., Fragneaud B., Marianetti C.A. et al.* // Phys. Rev. B. 2009. V. 80. № 20. P. 205407. https://doi.org/10.1103/PhysRevB.80.205407
44. *Cadelano E., Palla P.L., Giordano S. et al.* // Phys. Rev. B. 2010. V. 82. № 23. P. 235414. https://doi.org/10.1103/PhysRevB.82.235414
45. *Klintenberg M., Lebègue S., Ortiz C. et al.* // J. Phys.: Condens. Matter. 2009. V. 21. № 33. P. 335502. https://doi.org/10.1088/0953-8984/21/33/335502
46. *Lee C., Wei X., Kysar J.W. et al.* // Science. 2008. V. 321. № 5887. P. 385. https://doi.org/10.1126/science.1157996
47. *Kudin K.N., Scuseria G.E., Yakobson B.I.* // Phys. Rev. B. 2001. V. 64. № 23. P. 235406. https://doi.org/10.1103/PhysRevB.64.235406
48. *Peng Q., Ji W., De S.* // Comput. Mater. Sci. 2012. V. 56. P. 11. https://doi.org/10.1016/j.commatsci.2011.12.029
49. *Falin A., Cai Q., Santos E.J.G. et al.* // Nat. Commun. 2017. V. 8. № 1. P. 15815. https://doi.org/10.1038/ncomms15815
50. *Cooper R.C., Lee C., Marianetti C.A. et al.* // Phys. Rev. B. 2013. V. 87. № 3. P. 035423. https://doi.org/10.1103/PhysRevB.87.035423
51. *Bertolazz S., Brivio J., Kis A.* // ACS Nano. 2011. V. 5. № 12. P. 9703. https://doi.org/10.1021/nn203879f
52. *Steglenko D.V., Tkachenko N.V., Boldyrev A.I. et al.* // J. Comput. Chem. 2020. V. 41. № 15. P. 1456. https://doi.org/10.1002/jcc.26189
53. *Fedik N., Steglenko D.V., Muñoz-Castro A. et al.* // J. Phys. Chem. C. 2021. V. 125. № 31. P. 17280. https://doi.org/10.1021/acs.jpcc.1c02939
54. *Peng Q., Wen X., De S.* // RSC Adv. 2013. V. 3. № 33. P. 13772. https://doi.org/10.1039/c3ra41347k
55. *Şahin H., Cahangirov S., Topsakal M. et al.* // Phys. Rev. B. 2009. V. 80. № 15. P. 155453. https://doi.org/10.1103/PhysRevB.80.155453

56. *Ding J., Xu M., Guan P.F. et al.* // J. Chem. Phys. 2014. V. 140. № 6. P. 064501. https://doi.org/10.1063/1.4864106
57. *Sun J., Liu P., Wang M. et al.* // Sci. Rep. 2020. V. 10. № 1. P. 3408. https://doi.org/10.1038/s41598-020-60416-5

Table 1. Calculated Bravais lattice parameters, atomic coordinates and Wyckoff positions for $B_6Ga_2Mg_4$

Translation vectors, Å				
$\bar{a}$ = 5.2839		$\bar{c}$ = 13.3784		
atom	Wyckoff positions	atomic coordinates		
		x	*y*	*z*
Ga	2 *e*	0.00000	0.00000	0.64319
Mg	4 *h*	0.33333	0.66666	0.62737
B	6 *k*	0.33201	0.00000	0.50000

Table 2. Calculated values of elasticity constants (c_{ij}, N/m), Young's modulus (Y_{2D}, in N/m) and Poisson's ratio *v*

Compound	c_{11}	c_{12}	c_{66}	Y_{2D}	*v*
Graphene	358.0 [45]	55.0 [45]	152.0 [45]	340.0 ± 50 [46, 47]	0.149 [47]
2Dhex *hex* -BN	293.2 [48]	66.1 [48]	113.6 [48]	289 ± 24 [49]	0.218 [48]
2D-MoS_2	140.0 [50]	40.0 [50]	50.0 [50]	130 [50, 51]	0.290 [50]
2D-B_4P_2	142.5 [52]	2.5 [52]	13.6 [52]	142.5 [52]	0.017 [52]
2D-$B_6Ga_2Mg_4$	145.8	30.2	57.79	139.6	0.206
2D-B_4As_2	130.4 [53]	1.9 [53]	13.2 [53]	130.4 [53]	0.015 [53]
2D-B_2Na_2	107.1 [27]	8.36 [27]	49.35 [27]	106.4 [27]	0.078 [27]
Silicene	71.3 [54]	23.2 [54]	24.1 [54]	62 [55]	0.325 [54]

Table 3. Calculated energy values (in eV) of boron, gallium, magnesium atoms and two-dimensional $B_6Ga_2Mg_4$. Formation energy E_{f1} per formula unit (eV), E_{f2} per atom (eV/atom)

Compound	B	Ga	Mg	$B_6Ga_2Mg_4$	E_{f1}, eV	E_{f2}, eV/atom
Energy, eV	–0.337	–0.277	–0.001	–50.148	–47.57	–3.96

FIGURE CAPTIONS

Fig. 1. Structure of the two-dimensional system $B_6Ga_2Mg_4$. Boron atoms forming the honeycomb structure are shown in green, magnesium and gallium atoms in apical positions are shown in orange and light green, respectively: a - top view, b - side view.

Fig. 2. Top view and structure of the unit cell of the two-dimensional system $B_6Ga_2Mg_4$(a), side view of the surface fragment (b).

Fig. 3. Calculated dispersion curves of the phonon spectrum along the Γ–M–K–Γ path (a) and phonon density of states (b) for $B_6Ga_2Mg_4$.

Fig. 4. Electronic band structure of $B_6Ga_2Mg_4$ along the Γ–M–K–Γ path (a) and electronic density of states (b).

Fig. 5. Partial density of electronic states formed by boron atoms. The vertical dashed line indicates the Fermi level.

Fig. 6. Partial density of electronic states formed by gallium atoms. The vertical dashed line indicates the Fermi level.

Fig. 7. Partial density of electronic states formed by magnesium atoms. The vertical dashed line indicates the Fermi level.

Fig. 8. Pair correlation function (PCF) calculated for two-dimensional $B_6Ga_2Mg_4$ at various temperatures (a); surface fragment of size 4 × 4 × 1 at 1000 (b), 1200 (c), and 1300 K (d).

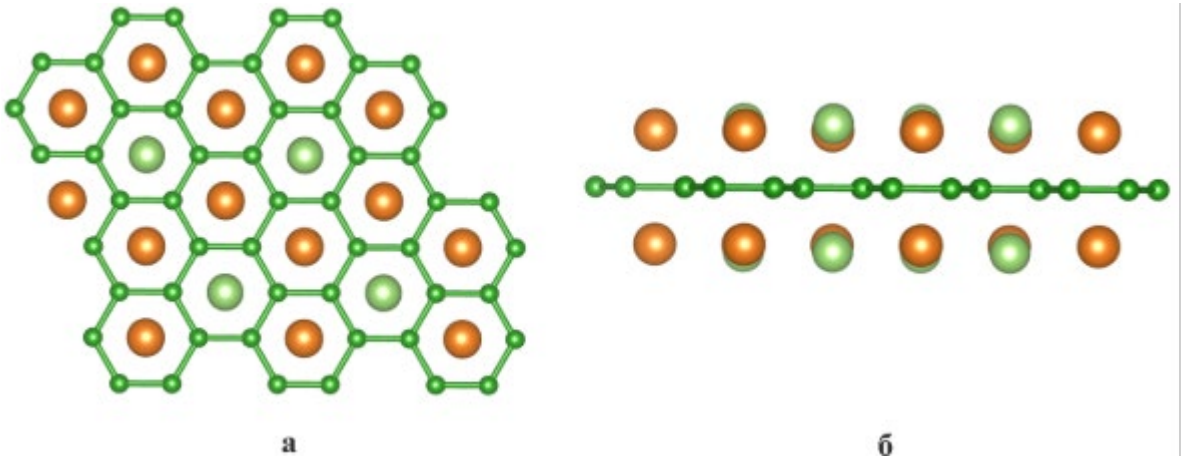

Fig. 1. Steglenko. a, b in brackets

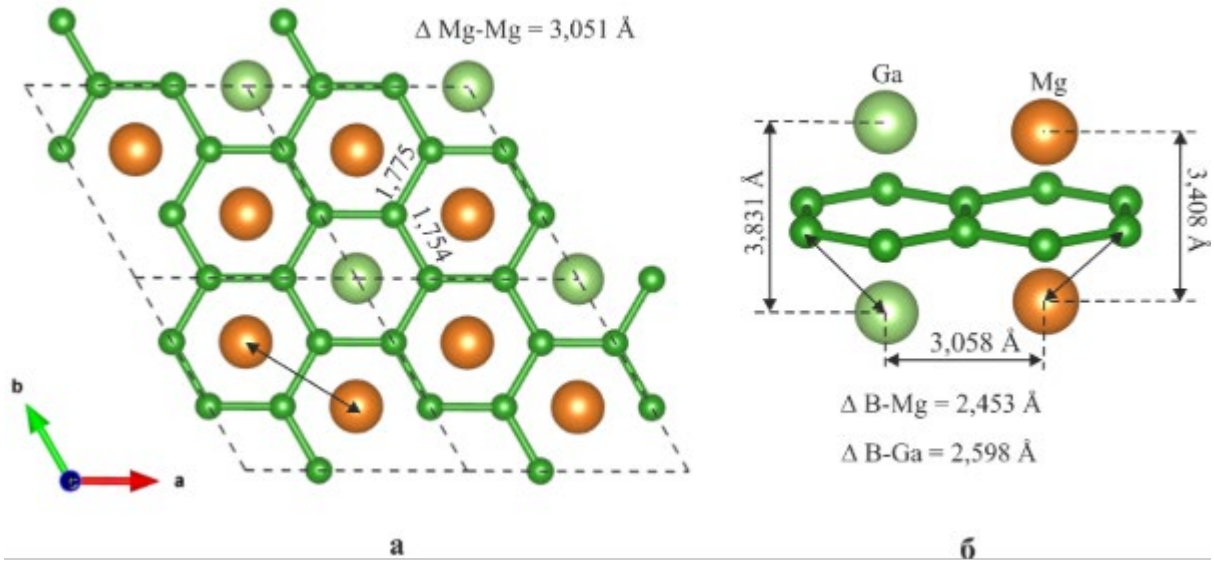

Fig. 2. Steglenko.

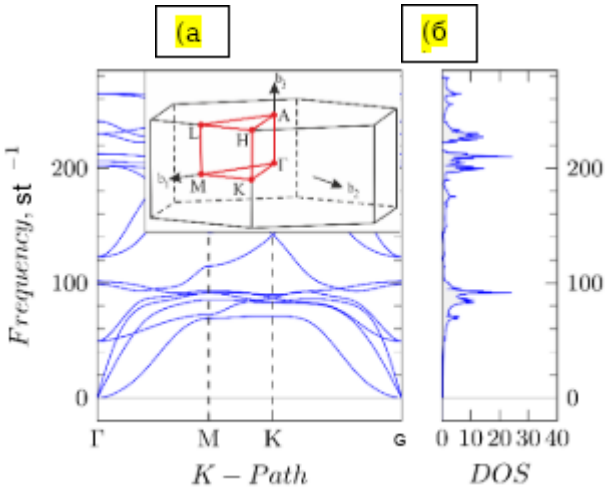

Fig. 3. Steglenko.

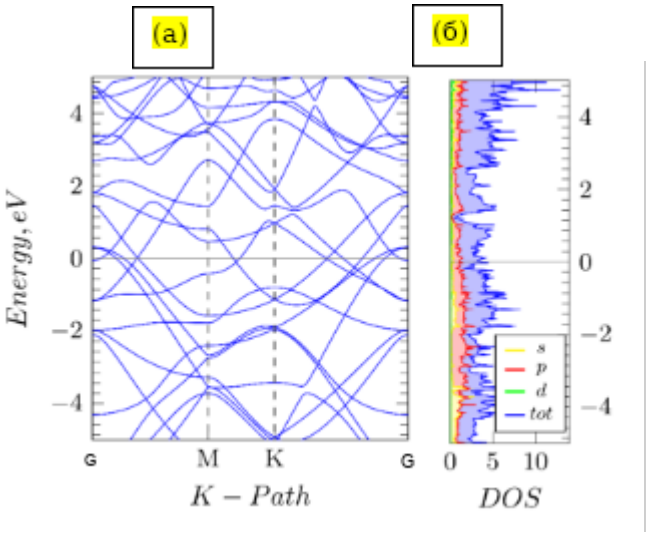

Fig. 4. Steglenko.

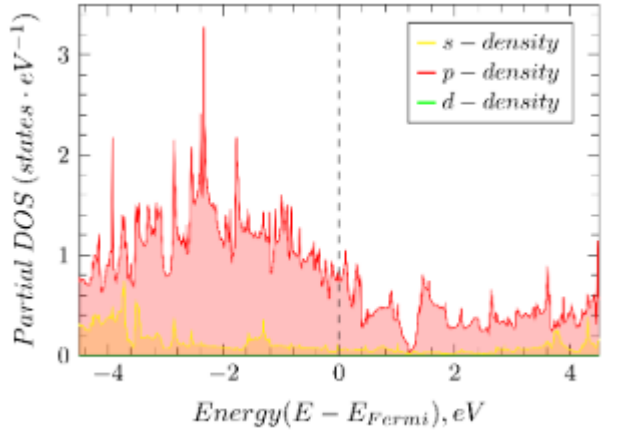

Fig. 5. Steglenko.

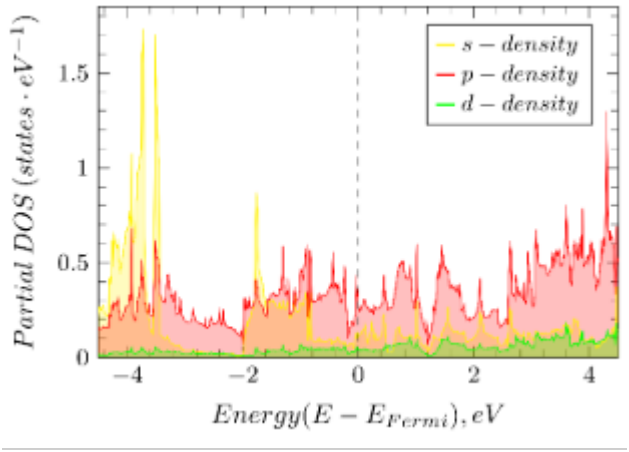

Fig. 6. Steglenko.

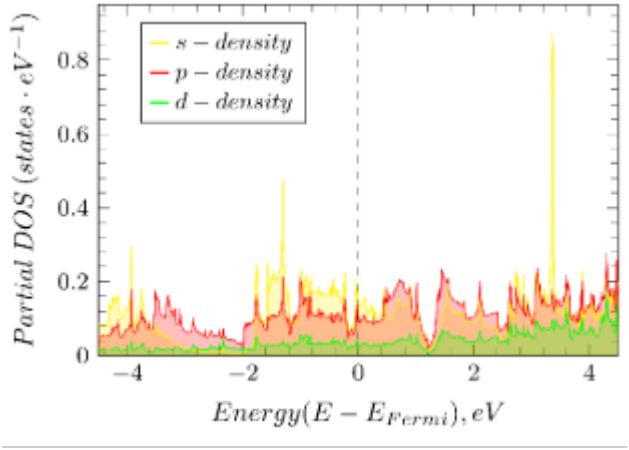

Fig. 7. Steglenko.

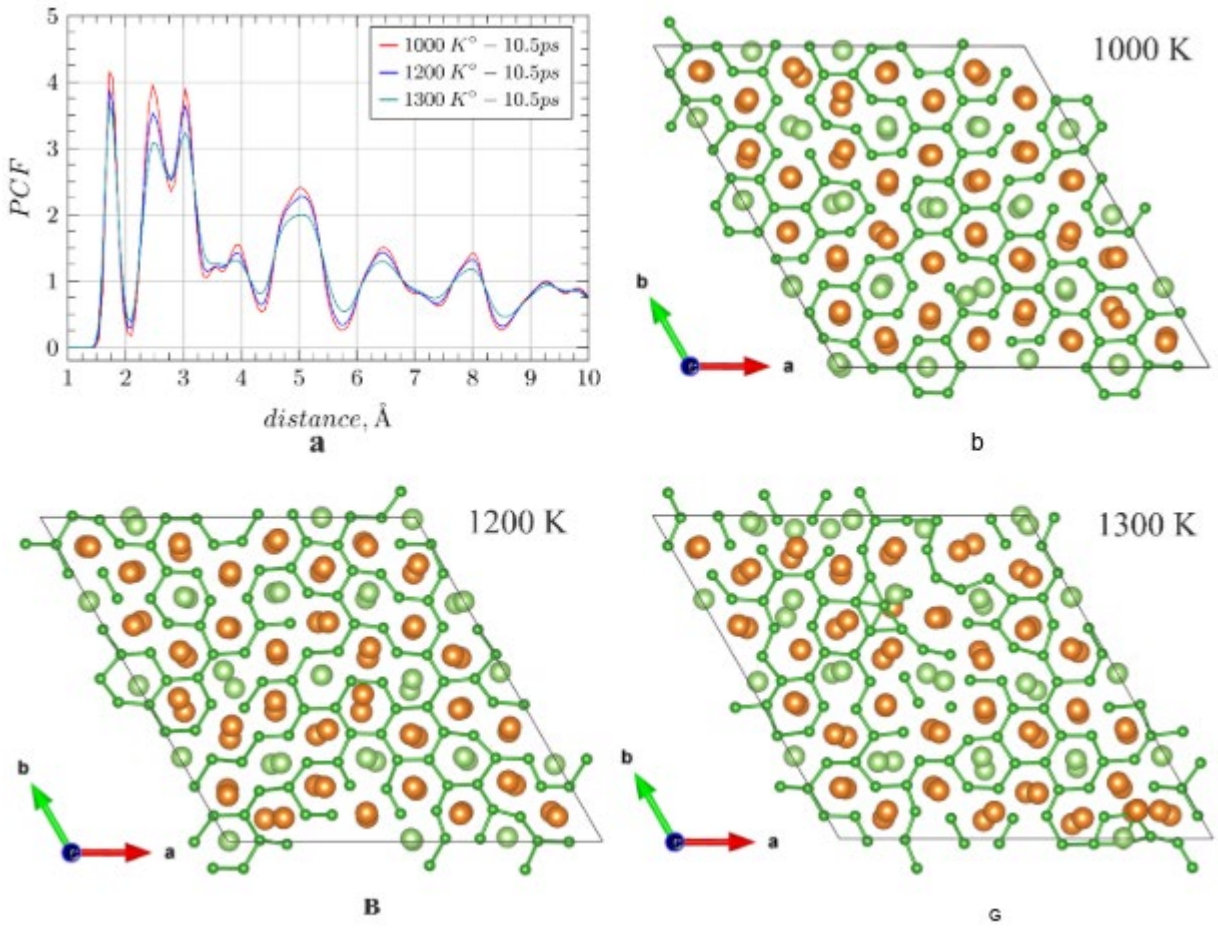

Fig. 8. Steglenko.